Suberosin alleviates thiazolidinedione-induced cardiomyopathy in diabetic rats by inhibiting ferroptosis via modulation of ACSL4-LPCAT3 and PI3K-AKT signaling pathways

Shabnoor Iqbal (shabnooriqbal@gcuf.edu.pk)
Government College University, Faisalabad

FARHAT Jabeen
Government College University, Faisalabad

Ivan Kahwa
Mbarara University of Science and Technology

Timothy Omara
University of Natural Resources and Life Sciences, Vienna (BOKU)

Research Article

Keywords: Thiazolidinediones, ferroptosis, cardiomyopathy, AKT, GSK3β, GPX4

Posted Date: June 26th, 2023

DOI: https://doi.org/10.21203/rs.3.rs-3061810/v1

Version of Record: A version of this preprint was published at Cardiovascular Toxicology on September 7th, 2023. See the published version at https://doi.org/10.1007/s12012-023-09804-7.

Abstract

Thiazolidinediones are antidiabetic medications that are useful for managing diabetes. However, their use is associated with adverse side effects like edema, heart failure, and bone fractures. In this study, we investigated the anti-ferroptosis effects of suberosin (SBR; a prenylated coumarin) in diabetic Sprague Dawley rats. Further, we assessed the effects of co-administration of SBR (30 and 90 mg/kg/day) with thiazolidinedione TZ (15 mg/kg) to mitigate TZ-induced cardiomyopathy in diabetic rats. Our results showed that cardiac output, stroke volume, left ventricle systolic, and diastolic pressure were aggravated in diabetic rats only treated with TZ after 4 weeks. TZ treatments were induced ferroptosis as well as marked histoarchitecture disarrangements in rat cardiomyocytes. The study was found that optimizing volume overload alleviated cardiac hypertrophy and mitigated left ventricular dysfunction in diabetic rats co-treated with SBR. SBR co-administration with TZ reduced MDA levels in heart tissue and serum iron concentration (biomarkers of ferroptosis) as well as downregulated mRNA expressions of LOX, ACSL4, LPCAT3, and promoted GPX4 activity as well as upregulated mRNA levels of AKT/PI3K/GSK3β in a dose-dependent manner as compared to the group administered with TZ at 15 mg/kg. SBR co-administration was also helped to retain the normal histoarchitecture of cardiomyocytes in diabetic rats. Hence, our results suggested that SBR is an effective supplement and could be prescribed to diabetic patients along with TZ but this will require further clinical trials.

Introduction

Diabetes mellitus is a carbohydrate metabolic disorder, usually resulting from impaired glucose homeostasis (Wild et al., 2004). The 2021 global diabetes prevalence raised up to 536 million cases and this might approach 783 million in 2045 (Sharma and Patial, 2022). Conversely, there is a correlation between cardiovascular ailments and fatalities or illnesses in individuals diagnosed with diabetes mellitus (Laing et al., 2003, Orasanu and Plutzky, 2009).

Thiazolidinediones (TZs) such as rosiglitazone and pioglitazone are currently being employed in the clinical management of diabetes mellitus. However, there seem to be increased risks of congestive heart failure and cardiac adverse effects as a result of the administration of TZs treatments (Juurlink et al., 2009). Nissen and Wolski were conducted a comprehensive meta-analysis which revealed that the administration of rosiglitazone was linked to heightened risks of cardiovascular death and myocardial infarction (Nissen and Wolski, 2007). However, subsequent studies have presented a diverse range of evidence regarding the risk of cardiovascular diseases in diabetic patients using rosiglitazone and pioglitazone. Antidiabetic therapies such as TZs that target peroxisome proliferator-activated receptor-gamma are required more comprehensive knowledge regarding their adverse effects (Lago et al., 2007, Rosen, 2007).

TZs have the potential to directly or indirectly cause cardiomyopathy. Research has demonstrated that rosiglitazone induces sodium reabsorption by upregulating renal tubule transporters, such as Atp1a1, Npt2, and NHE3, in the convoluted tubule, as well as Nkcc2 in ascending tubes of the kidney (Song et al.,

2004). The state of chronic volume overload is initially counteracted by cardiac hypertrophy; however, if the condition is not resolved, it ultimately results in cardiomyopathy and heart failure. Although, no such causative factors are known regarding TZs-induced cardiomyopathy and elevated plasma volume. To date, there is no experimental evidence indicating that the mitigation of TZs-induced congestive heart failure can be achieved through plasma volume release or the reduction of sodium reabsorption (Karalliedde et al., 2006, Rennings et al., 2011). Heart failure is distinguished by the presence of regulated cell death, autophagy, and ferroptosis. Ferroptosis is a type of programmed cell death that can be readily differentiated from other cellular mechanisms, including apoptosis, necroptosis, autophagy, and pyroptosis. (Guo et al., 2022). There is a need to explore natural products for their bioactivity for the management of side effects of TZ to lower the risk heart failure. The prenylated coumarin derivative (7-methoxy-6-(3-methylbut-2-enyl)bchromen-2-one), commonly known as suberosin (Fig. 1), is a natural product that has been previously isolated from the roots and aerial parts of *Cudrania tricuspidata*, *Ferulago carduchorum*, and *Prangos bucharica* (Kim et al., 2015, Karabulut Uzunçakmak et al., 2023). The potential of Suberosin (SBR) in the activation of trypsin, caspase- and chymotrypsin-like, and proteasome activities in a 20S proteasome activity assay has previously been reported to be dose-dependent (Kim et al., 2015). This current investigation targeted ferroptosis for managing TZs-induced cardiovascular conditions and to elucidate the anti-ferroptotic role of SBR when co-administered with TZs to reduce the risk of cardiomyopathy in diabetic rats.

Materials and methods

Chemicals and reagents

Thiazolidinedione (CAS 2295-31-0) utilized in the current investigation was procured from Sigma Aldrich, while the suberosin (CAS 581-31-7) was obtained from Cayman Chemical. The rest of the chemicals were of high analytical purity and were used without any further purification.

Ethical approval

The animal handling and treatment experimental protocols underwent review and monitoring by the ethical committee of the Government College University, Faisalabad, Pakistan. These protocols were following the approved protocol of the European Union of animal care and Experimentation (CEE Council 86/609). The research was conducted in adherence to the ARRIVE guidelines.

Streptozotocin-induced diabetes mellitus in rats

Diabetes was induced in Sprague Dawley rats by intraperitoneal injection (1 ml/kg of 50 mg/kg body weight (bw)) of citrate buffered streptozotocin (STZ). The STZ-treated rats were observed to have developed and achieved stabilization of diabetes for seven days. The control group were administered a pH 4.5 citrate buffer. After 1 week, the plasma glucose levels of the rats were determined. The study selected rats whose fasting plasma glucose levels ranged between 330-380 mg/dl (Latha and Daisy, 2011).

Assessment of suberosin toxicity

The subacute and acute toxicity of SBR was determined in Sprague Dawley rats with and without diabetes (150-200 g) following the OECD guideline 423 (Walum, 1998).

Experimental design

Thirty Sprague Dawley male rats (~100 g; 4 weeks old) were placed in clean steel cages at the animal house, following the approved animal handling and feeding protocol guidelines. The rats were allocated into five groups (n = 5) randomly. The cage temperature (25°C) and humidity (60-70%) were optimized, and the rats were provided with feeds and water *ad libitum*. The experiment was conducted for 28 days and all doses were administered orally. The SBR (30 and 90 mg/kg) and TZ (30 mg/kg) were given by oral gavage. For TZ, it was dissolved in deionized water and the standard dosage for people is 30 mg/kg of TZ delivered daily (Erdem Guzel et al., 2021). SBR was dissolved in deionized water and doses were selected after acute and sub-acute toxicity. All rats were treated for 4 weeks, under the following experimental groups.

NC-G1 group: Normal control rats received only water and feeds.

DC-G2 group: Diabetic control rats were received only water and feeds.

TZ-G3 group: TZ was administered orally at 30 mg/kg/day to diabetic rats.

SBR+TZ-G4 group: Diabetic rats were received SBR at 30 mg/kg/day and TZ (30 mg/kg/day) via oral gavage.

SBR+TZ-G5 group: Diabetic rats were co-administered SBR (90 mg/kg/day) and TZ (30 mg/kg/day) via oral gavage.

Volume analysis of blood plasma

Following anesthesia, 0.1 mL of Evans Blue dye (1 mg/mL) was injected via the portal vein. Subsequently, blood was collected from the vena cava after 3 minutes. The plasma volume was assessed by dividing the aggregate quantity of administered dye by the plasma dye concentration obtained through spectrophotometry (Chang et al., 2014).

Analysis of plasma sodium

The ARCHITECT c4000 Clinical Chemistry Analyze (Illinois, USA) was utilized to measure the concentrations of urinary sodium. The daily excretion of sodium was determined by multiplying the concentration of sodium with the volume of urine and subsequently dividing the product by the individual's body weight (Chang et al., 2014).

Iron assay

Iron concentration was determined by iron kit (abcam, ab239715). To prepare the serum, collected whole blood in a covered test tube placed on ice. The blood samples were vortexed to remove coagulation and retained the sample at ambient temperature, typically ranging from 15 to 30OC, and centrifuged at 1000 – 2000 x g for 10 minutes .and transferred the serum into a pristine polypropylene tube.

Malondialdehyde assay

The MDA concentrations were determined utilizing the same techniques as those utilized in the previous study conducted by Ohkawa et al. in 1979. Following centrifugation of the reaction mixture at a rate of 4000 revolutions per minute for 10 minutes, the absorbance of the supernatant was assessed at a wavelength of 532 nanometers. The study was presented the data in terms of nanomolar concentrations per gram of tissue.(Ohkawa et al., 1979).

Assessment of Echocardiography

The rats were anesthetized with isoflurane. Acquisition of echocardiographic images was achieved using a Vevo 770 microimaging system with a 25-MHz probe (Visual Sonics, Toronto, ON, Canada). The left ventricle (LV) was imaged using parasternal short-axis views at the papillary muscle level, and M-mode recordings were collected. The study conducted diastolic measurements at the location of the greatest cavity dimension, while systolic measurements were taken at the point of minimal cavity dimension, utilizing the leading edge method (Schiller et al., 1989).

cDNA synthesis

After assessment of the amount and integrity of the entire RNA sample from heart tissue and made solution by combining 5 µg of total RNA with 10 µL volume, along with 1 µL of oligo (dT) primer and 1 µL of random hexamer primer. Subsequently, the blend was subjected to incubation at a temperature of 70 °C for 300 seconds, expeditiously cooled on ice, and augmented with 0.5 µL of RNase inhibitor (40 U/µL), 1 µL of 10 mM deoxyribonucleoside triphosphates, 4 µL of quintuple first-strand buffer and 1 µL of reverse transcriptase (Moloney Murine Leukemia Virus) (Bahari et al., 2017).

Quantitative reverse transcription polymerase chain reaction (RT-qPCR)

The experimental procedure involved the combination of 0.5 µL of both forward and reverse primers (Table 1) for the genes PI3K, AKT, GSK3β, LPCAT3, ACSL4, LOX, GPX4, and β-actin (utilized as a house-keeping gene), with cDNA (1 µL), SYBR Green qPCR Mix 2X (10 µL), and nuclease-free water (8 µL), resulting in a 20 µL reaction volume in a 0.2 mL thin-walled PCR microtube. The study was carried out following the QuantiTect Rev. Transcription Kit protocol utilizing the Rotor-Gene® Q qPCR (QIAGEN®) instrument. The Rotor-Gene Software was employed to conduct the cycling process, which consisted of an initial holding phase at 95 °C for 10 minutes, followed by 40 cycles of denaturation (at 95 °C for 10 seconds), annealing (at 60 °C for 15 seconds), and extension (at 72 °C for 20 seconds). The process concluded with a final extension step at 72°C for 10 minutes. Following this, a secondary incubation was performed at a temperature of 95°C for one minute. Furthermore, a gradual temperature increase ranging

from 54°C to 95°C was implemented for approximately 3 to 4 minutes to execute the melting process. Following the amplification of each PCR product, a melting curve analysis was performed which yielded a single peak (Mohammadi et al., 2014, Rassouli et al., 2022).

Table 1. Primer sequences used for the RT-qPCR

Target gene	Primers 5’ -> 3	Accession number
Akt	Forward: 5’- GCACCGTGTGACCATGAACG -3”	XM_006240631.3
	Reverse: 5'- AGTAAGCGTGTGGGCAACCT -3'	
PI3K	Forward: 5'-TTACGGCGGCATGGGAATCT-3'	XM_017595947.2
	Rerverse:5'-CCAGCTTTCCCTGAGTGCCT-3	
GSK3β	Forward: 5’- CCTCGGGACGAGGAAGAAGAG -3	NM_001014198.2
	Reverse 5’- ACGTCATTGACAACGGCCTC -3’	
LPCAT3	Forward: 5’- AGCCTTAACAAGTTGGCGACG-3’	NM_001012189.1
	Reverse: 5’- AGTGGTAGAACTGGTGGCCG-3’	
GPX4	Forward 5’- GCCGTCTGAGCCGCTTATTG-3’	NM_017165.4
	Reverse 5’- TGCGAATTCGTGCATGGAGC-3’	
ACSL4	Forward: 5’-ACAGAATCATGCGGTGCTGGA-3’	XM_006257315.4
	Reverse: 5’- ACAGCAAATAAGAGGAGCGCCA-3’	
LOX	Forward: 5’- TGCCTGGCCAGTTCAGCATA-3’	XM_006254715.4
	Reverse:5’- ATCCAGCAGGTCGTAGTGGC-3’	
β-actin	Forward: 5’ -CGCGAGTACAACCTTCTTGCAG-3’	NM_031144.3
	Reverse 5’- CGCAGCGATATCGTCATCCA-3’	

Histological analysis

The heart tissues underwent standard paraffin processing, involving a series of steps such as dehydration (in 70%, 95%, and absolute alcohol), clearance in xylene, and infiltration at 70°C for 2 hours each. Subsequently, the tissues were subjected to paraffin wax embedding and sliced into sections of 5 µm thickness. The specimens were subjected to hematoxylin and eosin staining before histopathological examination (Wittekind, 2003).

Statistical analysis

Obtained data were subjected to one-way or two-way analysis of variance and unpaired two-tailed test followed by Tukey's posthoc test in GraphPad Prism for Windows (v5, GraphPad Software, USA). The means were considered to be statistically significant where $P < 0.05$, or $P<0.01$.

Results

Toxicity assessment results

The outcomes of the acute toxicity test on SBR indicated that its median lethal dose (LD_{50}) is >2000 mg/kg, hence it is safe to use for rats. For SBR subacute toxicity in rats at 30 mg/kg and 90 mg/kg, the complete blood chemistry, liver, and kidney function tests, and histology results indicated that it is safe after 4 weeks of administration. During the experiment, the rats were observed daily but only slight alterations in behavior were noted and could not be attributed directly to toxicity of SBR.

SBR mitigates TZ-induced volume expansion and ventricle dysfunction

In this, rats were co-administered with SBR (@30 mg/kg and 90 mg/kg/day) and TZ (@15 mg/kg/day) to mitigate volume expansion and investigated whether it is a causative factor in TZ-induced heart weight gain and observed heart function by electrocardiographic measurements. Following four weeks of co-treatment with SBR and TZ, fractional shortening (FS), ejection fraction (EF), left ventricular systolic diameter (LVDs), left ventricular diastolic diameter (LVDd), left ventricular end-systolic volume (LVEVs), and left ventricular end-diastolic volume (LVEVd), stroke volume, and cardiac output were optimized than only TZ treated rats (**Fig. 2**).

The co-administration of SBR and TZ were improved the TZ-mediated reduction of hematocrit, reduction of plasma volume/BW as well as a decrease in urine sodium/BW and HW/BW than TZ-G3 group in a dose-dependent manner (**Fig. 3**).

Co-administration of SBR with TZ alleviates biomarkers of ferroptosis (total iron concentration and lipid peroxidation)

SBR co-administration with TZ was reinstated the levels of oxidation by-product malondialdehyde (MDA) and optimized total iron concentration ($P < 0.001$) than only TZ treated group after 4 weeks of treatments, while groups treated with TZ for 4 weeks were showed a significantly high total iron and MDA levels (**Fig. 4**).

SBR modulates TZ-induced mediators of ferroptosis (ACSL4 -LPCAT3 and PI3K-AKT signaling pathways)

The mRNA levels of ferroptosis mediators LOX, LPCAT3, ACSL4, and GPX4 and AKT, PI3K, and GSK-3β were determined by RT-qPCR following a four-week administration of TZ with or without SBR were assessed. Induction by TZ resulted in significant upregulation of mRNA levels of ACSL4, LOX, and LPCAT3, while simultaneously downregulated mRNA expressions of AKT, PI3K, and GSK3β ($P<0.01$, $P<0.001$) in a dose-response manner. The findings of our study indicate a statistically significant

decrease in ferroptotic inducers (P<0.01, P<0.001) (P<0.01, P<0.001) in co-administered SBR-G3 and SBR-G4 groups, as compared to the TZ-G2 group (**Fig. 5**).

Anti-ferroptosis activity of SBR suppressed TZ-induced necrosis and disarrangement of cardiac tissues

The heat histoarchitecture obtained showed that there was significant damage in rats that were administered with TZ only (**Fig. 6**; C). In addition, marked necrosis, wavy arrangements and hypereosinophilia were evident. Conversely, the normal histoarchitecture of the heart was observed in control rats (**Fig. 6** A and B). The administration of SBR at low and high doses resulted in the restoration of normal histoarchitecture in rats when co-administered with TZ in dose dependent-manner (**Fig. 6** D and E).

Discussion

Investigation of the toxicity of natural products is important before their use in the development of drugs. In this study, SBR had LD50 >2000 mg/kg, hence it is safe in rats. Though data on the toxicity of this compound is scarce, an extract of Ferulago carduchorum containing SBR was previously reported to be safe (LD50 >2000 mg/kg) (Golfakhrabadi et al., 2014).

Regarding the effects of SBR on TZ-induced cardiomyopathy, investigation of diverse pathophysiological mechanisms and gene regulations was done for 4 weeks. Echocardiography is a widely recognized and minimally invasive diagnostic technique utilized in clinical settings to precisely assess myocardial dysfunction, cardiac anatomy, and hemodynamic function (Xu et al., 2009). A previous study stated that the cause of TZ-induced cardiac hypertrophy was either an elevation in plasma volume or a modification in cardiac nutrient preference (Chang et al., 2014). The current study depicted that releasing volume overload after administration of SBR (@ 30 and 90mg/kg/day) for 4 weeks were optimized TZ-induced cardiac hypertrophy, and left ventricle dysfunction by regulating target factors of the study including ejection fraction; fractional shortening, left ventricular systolic diameter, and diastolic diameter, end-systolic volume, and end-diastolic volume. Consequently, the effects observed in TZ treatments have been attributed to the volumetric expansion, which led to adverse effects on the cardiac tissue. Co-administration of SBR with TZ regulated ventricle function by reducing systolic and diastolic diameter, stroke volume, as well as end stroke volume of the left ventricle. Other physiological parameters (including plasma volume/BW, heart weight/BW, hematocrit, and urine sodium/ BW) were improved after SBR co-administration with TZ and this occurred in a rather dose-dependent manner. The results we obtained are similar to previous study examining the therapeutic effectiveness of osthol (a coumarin derivative isolated from Cnidium monnieri fruits) in treating cardiac hypertrophy in rats where rats treated with osthol exhibited a significant effect on both systolic and diastolic blood pressure as well as heart weight index (Zhou et al., 2012).

The administration of TZs led to the activation of sodium reabsorption by inducing the upregulation of different renal tubule transporters, specifically in the proximal convoluted tubule and the thick ascending limb. Furthermore, research has shown that the activation of renal peroxisome proliferator-activated

receptor gamma leads to the upregulation of the epithelial sodium channel (ENaCg), a subunit of the sodium transporter situated in the collecting duct (Sharma and Patial, 2022). The augmentation of renal sodium transporters leads to an elevation in sodium reabsorption, which consequently induces an increase in volume expansion. Cardiac hypertrophy serves as an initial compensatory mechanism to counterbalance the state of chronic volume overload. If the medical condition persists, it can ultimately lead to the development of cardiomyopathy and subsequent heart failure (Horita et al., 2015). TZ-only treated rats were observed with aggravated levels of plasma volume/BW, HW/BW, and urine sodium. This effect may be attributed to an augmented collagen breakdown and a reduction in lysine residue glycation on collagen in the left ventricle. These findings suggest a positive correlation between effective diabetic management and the amelioration of cardiac hypertrophy (Patel and Goyal, 2011) In the present study, administration of SBR (@30mg/kg and 90mg/kg) were improved the plasma volume/BW and HW/BW, the optimized level of urine sodium, and serum total iron and MDA levels. Ferroptosis is a form of controlled cellular demise that is primarily facilitated by lipid peroxidation that is dependent on iron, as evidenced by scholarly research (Xu, 2019). The manifestation of ferroptosis is distinguished by the anomalous configuration of mitochondria and the heightened concentrations of iron and lipid hydroperoxides (Dixon et al., 2012b). The overabundance of iron stimulates the production of reactive oxygen species (ROS) through the Fenton reaction and expedites the process of lipid peroxidation, as evidenced by previous research (Hua et al., 2020). Liang et al. was found coumarin derivative (skimm) assisted to restored alteration in plasma volume and heart weight in diabetic rats by preventing ferroptosis and autophagy as well as reducing oxidative stress (Liang et al., 2021). The induction of ferroptosis is multifactorial (includes specific small molecules or conditions that hinder the synthesis of glutathione or the efficacy of the glutathione peroxidase 4 (GPX4) enzyme) and is liable on glutathione (Cao and Dixon, 2016). Subsequent studies have indicated that altered iron metabolism, decreased levels of glutathione, inactivation of GPX4, and increased peroxidation of polyunsaturated fatty acids (PUFAs) by reactive oxygen species are crucial factors in the onset and advancement of ferroptosis (Dixon et al., 2012a, Stockwell et al., 2017). Participation of acyl-CoA synthetase long-chain family member 4 (ACSL4) is also cited as essential for ferroptosis because it aids the creation of PUFAs (Doll et al., 2017). Lipoxygenases (LOXs) are a class of enzymatic proteins that contain iron and catalyze the deoxygenation of PUFAs, and thus are involved in ferroptosis (Singh and Rao, 2019) and sn2-15-hydroperoxy-eicasotetraenoyl-phosphatidylethanolamines (sn2-15-HpETE-PE) generated by 15-LOX are regarded as a marker of ferroptosis (Anthonymuthu et al., 2018). However, the mechanisms of ferroptosis in the process of lipid peroxidation take place on esterified PUFAs-PLs rather than on free PUFAs (Dixon et al., 2015, Li et al., 2015). The present findings were showed TZ treatment induced ferroptosis, which was attributed to the upregulated mRNA expressions of LOX, ACSL4, and LPCAT3 and downregulated GPX4 expression. However, co-administration of SBR with TZ was found to optimize the relative mRNA expressions. The findings of the previous investigation have demonstrated that psoralidin, a coumarin compound, displays anti-ferroptosis effectiveness in both in vivo and in vitro. It can be presumed from the available evidence that natural compounds exhibit inhibitory effects on ferroptosis, thereby facilitating their anti-diabetic properties. Conversely, these compounds promote ferroptosis to effectively manage cancer and liver fibrosis (Yang et al., 2017), these findings support our study.

The present investigation demonstrated upregulated AKT-PI3K signaling and downregulated ferroptosis inducer pathway ASCL4-LCAT3 upon co-administration of SBR with TZ to mitigate the incidence of cardiomyopathy in rats with diabetes. The study conducted by de Oliveira et al. revealed that carnosic acid (a coumarin derivative like SBR in this study) had a mitigating effect on methylglyoxalin-induced ferroptosis in neuroblastoma cells. This was accomplished through the activation of the PI3K/Akt/Nrf2 signaling pathway and the modulation of antioxidant enzymes by the Nrf2 transcription factor (de Oliveira et al., 2015), which could be the case in the present anti-autophagy effect of SBR.

Conclusion

The onset of cardiomyopathy in rats with diabetes was caused by TZ. However, the co-administration of SBR with TZ was found to be effective in reducing the risk of cardiomyopathy. This was achieved by suppressing ferroptosis and maintaining physiological parameters related to heart function, such as left ventricle systolic and diastolic diameter volume, stroke volume, and cardiac output. Suberosin might be used as a supplement that could be prescribed to diabetic patients who are recommended to take thiazolidinedione, to reduce the risk of cardiomyopathy but this will require further clinical trials.

Abbreviations

LPCAT3; Lysophosphatidylcholine Acyltransferase 3

ACSL4; Acyl coenzyme A synthetase long-chain member 4

LOX; Lysyl oxidase

GPX4; Glutathione peroxidase 4

AKT; Protein Kinase B

PI3K; Phosphoinositide 3-kinase

GSK3β; Glycogen Synthase Kinase-3 Beta

Declarations

The authors claim that they do not have any apparent financial conflicts of interest that may have potentially influenced the findings presented in this manuscript.

Ethical Approval

The experimental procedure received approval from the Local Animal Ethical Committee of Government College University, Faculty of Zoology, and all stages of the investigation were authorized according to ethical guidelines.

Competing interests

The author declares no competing interests.

Authors' contributions

Shabnoor Iqbal: Investigation, Writing of Original Draft; **Farhat Jabeen: Supervision,** Validation and Writing; **Ivan Kahwa:** Data analysis; **Timothy Omara**: Review and editing.

Funding

No funding available

Availability of data and materials

The data is available upon request from the authors if reasonable.

References

1. Anthonymuthu TS, Kenny EM, Shrivastava I, Tyurina YY, Hier ZE, Ting H-C, Dar HH, Tyurin VA, Nesterova A, Amoscato AA (2018) Empowerment of 15-lipoxygenase catalytic competence in selective oxidation of membrane ETE-PE to ferroptotic death signals, HpETE-PE. J Am Chem Soc 140: 17835–17839
2. Bahari S, Zeighami H, Mirshahabi H, Roudashti S, Haghi F (2017) Inhibition of Pseudomonas aeruginosa quorum sensing by subinhibitory concentrations of curcumin with gentamicin and azithromycin. Journal of global antimicrobial resistance 10: 21–28
3. Cao JY, Dixon SJ (2016) Mechanisms of ferroptosis. Cell Mol Life Sci 73: 2195–2209
4. Chang C-S, Tsai P-J, Sung J-M, Chen J-Y, Ho L-C, Pandya K, Maeda N, Tsai Y-S (2014) Diuretics prevent thiazolidinedione-induced cardiac hypertrophy without compromising insulin-sensitizing effects in mice. The American Journal of Pathology 184: 442–453
5. de Oliveira MR, Ferreira GC, Schuck PF, Dal Bosco SM (2015) Role for the PI3K/Akt/Nrf2 signaling pathway in the protective effects of carnosic acid against methylglyoxal-induced neurotoxicity in SH-SY5Y neuroblastoma cells. Chem Biol Interact 242: 396–406
6. Dixon SJ, Lemberg KM, Lamprecht MR, Skouta R, Zaitsev EM, Gleason CE, Patel DN, Bauer AJ, Cantley AM, Yang WS (2012a) Ferroptosis: an iron-dependent form of nonapoptotic cell death. Cell 149: 1060–1072
7. Dixon SJ, Winter GE, Musavi LS, Lee ED, Snijder B, Rebsamen M, Superti-Furga G, Stockwell BR (2015) Human haploid cell genetics reveals roles for lipid metabolism genes in nonapoptotic cell death. ACS Chem Biol 10: 1604–1609
8. Doll S, Proneth B, Tyurina YY, Panzilius E, Kobayashi S, Ingold I, Irmler M, Beckers J, Aichler M, Walch A (2017) ACSL4 dictates ferroptosis sensitivity by shaping cellular lipid composition. Nat Chem Biol

13: 91–98

9. Erdem Guzel E, Kaya Tektemur N, Tektemur A, Etem Onalan E (2021) Carbamazepine-induced renal toxicity may be associated with oxidative stress and apoptosis in male rat. Drug Chem Toxicol: 1–8
10. Golfakhrabadi F, Abdollahi M, Ardakani MRS, Saeidnia S, Akbarzadeh T, Ahmadabadi AN, Ebrahimi A, Yousefbeyk F, Hassanzadeh A, Khanavi M (2014) Anticoagulant activity of isolated coumarins (suberosin and suberenol) and toxicity evaluation of Ferulago carduchorum in rats. Pharm Biol 52: 1335–1340
11. Guo Y, Zhang W, Zhou X, Zhao S, Wang J, Guo Y, Liao Y, Lu H, Liu J, Cai Y, Wu J, Shen M (2022) Roles of Ferroptosis in Cardiovascular Diseases. Front Cardiovasc Med 9: 911564
12. Horita S, Nakamura M, Satoh N, Suzuki M, Seki G (2015) Thiazolidinediones and Edema: Recent Advances in the Pathogenesis of Thiazolidinediones-Induced Renal Sodium Retention. PPAR Research 2015: 646423
13. Hua Z, Ma K, Liu S, Yue Y, Cao H, Li Z (2020) LncRNA ZEB1-AS1 facilitates ox-LDL-induced damage of HCtAEC cells and the oxidative stress and inflammatory events of THP-1 cells via miR-942/HMGB1 signaling. Life Sci 247: 117334
14. Juurlink DN, Gomes T, Lipscombe LL, Austin PC, Hux JE, Mamdani MM (2009) Adverse cardiovascular events during treatment with pioglitazone and rosiglitazone: population based cohort study. BMJ 339: b2942
15. Karabulut Uzunçakmak S, Halıcı Z, Karakaya S, Kutlu Z, Sağlam YS, Bolat İ, Aydın P, Kılıç CS (2023) Suberosin Alleviates Sepsis-Induced Lung Injury in A Rat Model of Cecal Ligation and Puncture. J Invest Surg 36: 2136802
16. Karalliedde J, Buckingham R, Starkie M, Lorand D, Stewart M, Viberti G (2006) Effect of various diuretic treatments on rosiglitazone-induced fluid retention. J Am Soc Nephrol 17: 3482–3490
17. Kim B-H, Kwon J, Lee D, Mar W (2015) Neuroprotective Effect of Demethylsuberosin, a Proteasome Activator, against MPP+-induced Cell Death in Human Neuroblastoma SH-SY5Y Cells. Planta Medica Letters 2: e15-e18
18. Lago RM, Singh PP, Nesto RW (2007) Congestive heart failure and cardiovascular death in patients with prediabetes and type 2 diabetes given thiazolidinediones: a meta-analysis of randomised clinical trials. The Lancet 370: 1129–1136
19. Laing S, Swerdlow A, Slater S, Burden A, Morris A, Waugh NR, Gatling W, Bingley P, Patterson C (2003) Mortality from heart disease in a cohort of 23,000 patients with insulin-treated diabetes. Diabetologia 46: 760–765
20. Latha RCR, Daisy P (2011) Insulin-secretagogue, antihyperlipidemic and other protective effects of gallic acid isolated from Terminalia bellerica Roxb. in streptozotocin-induced diabetic rats. Chem Biol Interact 189: 112–118
21. Li Z, Jiang H, Ding T, Lou C, Bui HH, Kuo M-S, Jiang X-C (2015) Deficiency in lysophosphatidylcholine acyltransferase 3 reduces plasma levels of lipids by reducing lipid absorption in mice. Gastroenterology 149: 1519–1529

22. Liang RK, Zhao YY, Shi ML, Zhang G, Zhao YJ, Zhang BG, Liang RJ (2021) Skimmin protects diabetic cardiomyopathy in streptozotocin-induced diabetic rats. Kaohsiung J Med Sci 37: 136–144
23. Mohammadi A, Mehrzad J, Mahmoudi M, Schneider M (2014) Environmentally relevant level of aflatoxin B1 dysregulates human dendritic cells through signaling on key toll-like receptors. Int J Toxicol 33: 175–186
24. Nissen SE, Wolski K (2007) Effect of rosiglitazone on the risk of myocardial infarction and death from cardiovascular causes. N Engl J Med 356: 2457–2471
25. Ohkawa H, Ohishi N, Yagi K (1979) Assay for lipid peroxides in animal tissues by thiobarbituric acid reaction. Anal Biochem 95: 351–358
26. Orasanu G, Plutzky J (2009) The pathologic continuum of diabetic vascular disease. J Am Coll Cardiol 53: S35-S42
27. Patel SS, Goyal RK (2011) Cardioprotective effects of gallic acid in diabetes-induced myocardial dysfunction in rats. Pharmacognosy Res 3: 239
28. Rassouli A, Shihmani B, Mehrzad J, Shokrpoor S (2022) The immunomodulatory effect of minocycline on gene expression of inflammation related cytokines in lipopolysaccharide-treated human peripheral blood mononuclear cells. Anim Biotechnol: 1–7
29. Rennings A, Russel F, Li Y, Deen P, Masereeuw R, Tack C, Smits P (2011) Preserved Response to Diuretics in Rosiglitazone-Treated Subjects With Insulin Resistance: A Randomized Double-Blind Placebo-Controlled Crossover Study. Clin Pharmacol Ther 89: 587–594
30. Rosen CJ (2007) The rosiglitazone story—lessons from an FDA Advisory Committee meeting. N Engl J Med 357: 844–846
31. Schiller NB, Shah PM, Crawford M, DeMaria A, Devereux R, Feigenbaum H, Gutgesell H, Reichek N, Sahn D, Schnittger I (1989) Recommendations for quantitation of the left ventricle by two-dimensional echocardiography. J Am Soc Echocardiogr 2: 358–367
32. Sharma V, Patial V (2022) Peroxisome proliferator-activated receptor gamma and its natural agonists in the treatment of kidney diseases. Front Pharmacol 13: 991059
33. Singh NK, Rao GN (2019) Emerging role of 12/15-Lipoxygenase (ALOX15) in human pathologies. Prog Lipid Res 73: 28–45
34. Song J, Knepper MA, Hu X, Verbalis JG, Ecelbarger CA (2004) Rosiglitazone activates renal sodium- and water-reabsorptive pathways and lowers blood pressure in normal rats. J Pharmacol Exp Ther 308: 426–433
35. Stockwell BR, Angeli JPF, Bayir H, Bush AI, Conrad M, Dixon SJ, Fulda S, Gascón S, Hatzios SK, Kagan VE (2017) Ferroptosis: a regulated cell death nexus linking metabolism, redox biology, and disease. Cell 171: 273–285
36. Walum E (1998) Acute oral toxicity. Environ Health Perspect 106: 497–503
37. Wild S, Roglic G, Green A, Sicree R, King H (2004) Global prevalence of diabetes: estimates for the year 2000 and projections for 2030. Diabetes Care 27: 1047–1053

38. Wittekind D (2003) Traditional staining for routine diagnostic pathology including the role of tannic acid. 1. Value and limitations of the hematoxylin-eosin stain. Biotech Histochem 78: 261–270
39. Xu J, Zhang C, Khanna A (2009) Wideband High-Frequency Echocardiography to Evaluate Myocardial Infarct Size. J Ultrasound Med 28: 1527–1534
40. Xu S (2019) Iron and Atherosclerosis: The Link Revisited. Trends Mol Med 25: 659–661
41. Yang C, Ma X, Wang Z, Zeng X, Hu Z, Ye Z, Shen G (2017) Curcumin induces apoptosis and protective autophagy in castration-resistant prostate cancer cells through iron chelation. Drug Des Devel Ther: 431–439
42. Zhou F, Zhong W, Xue J, Gu ZL, Xie ML (2012) Reduction of rat cardiac hypertrophy by osthol is related to regulation of cardiac oxidative stress and lipid metabolism. Lipids 47: 987–994

Figures

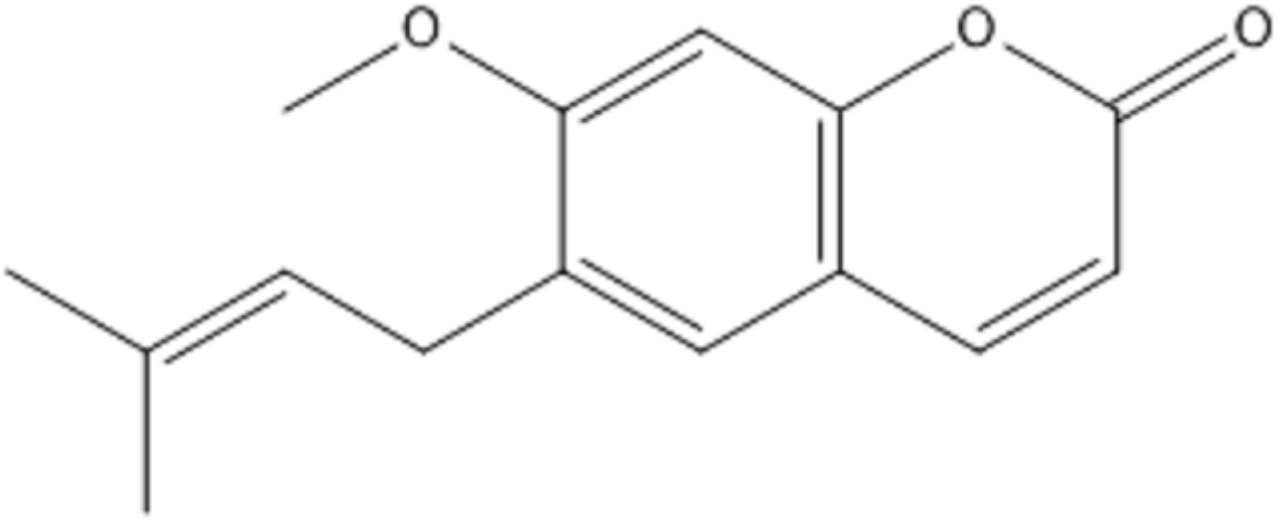

Figure 1

Chemical structure of suberosin

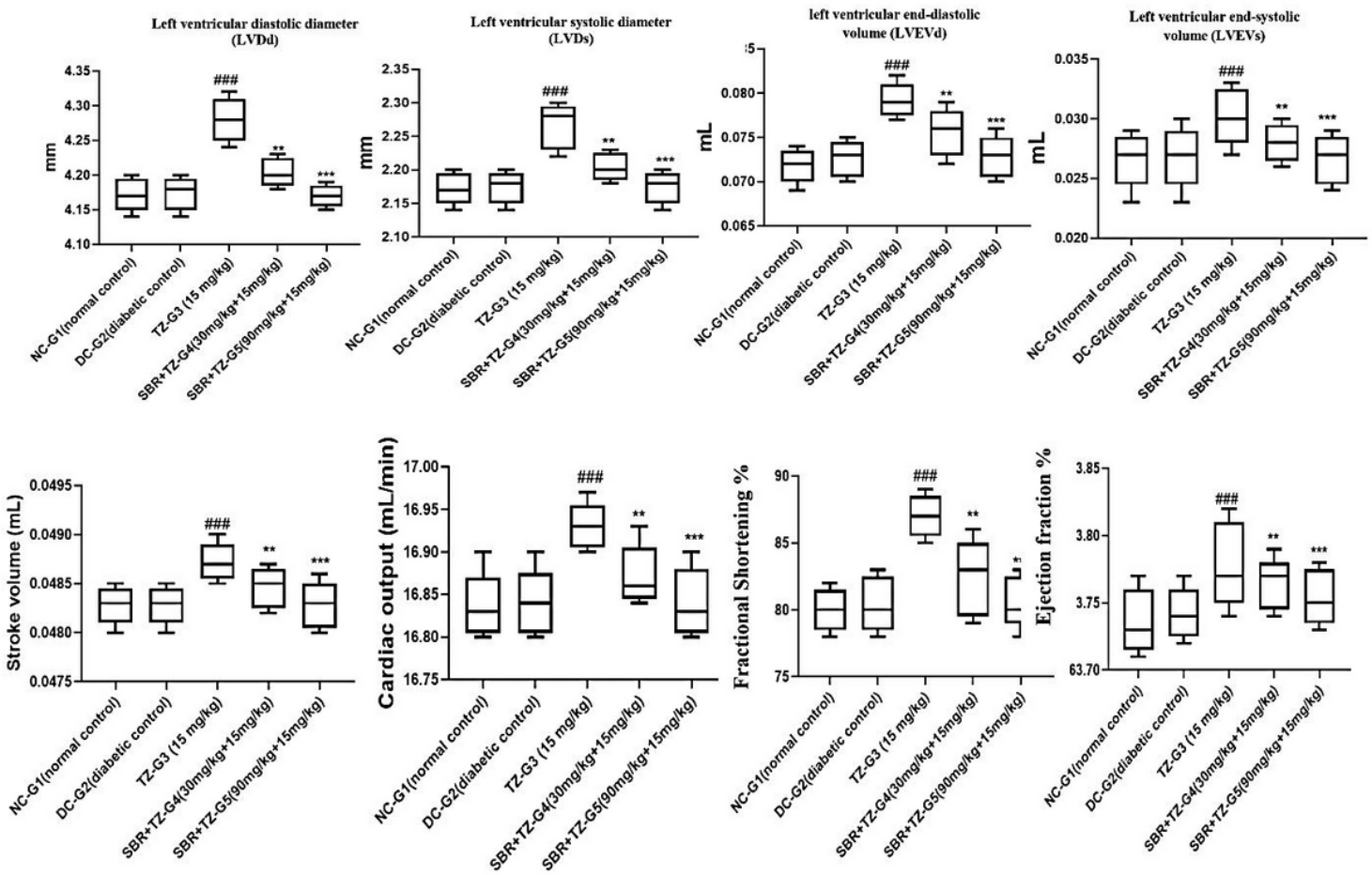

Figure 2

Effect of co-treatment of SBR and TZ on the improved LDVd, LVDs, LVEVd, LVEVs, stroke volume, cardiac output, ejection fraction, and fraction shortening of rats.

Values are stated as means ± standard deviations of replicates, ** P < 0.01, *** P< 0.001 compared with the TZ-G3 group. ### P < 0.001 compared with NC-G1 & DC-G2.

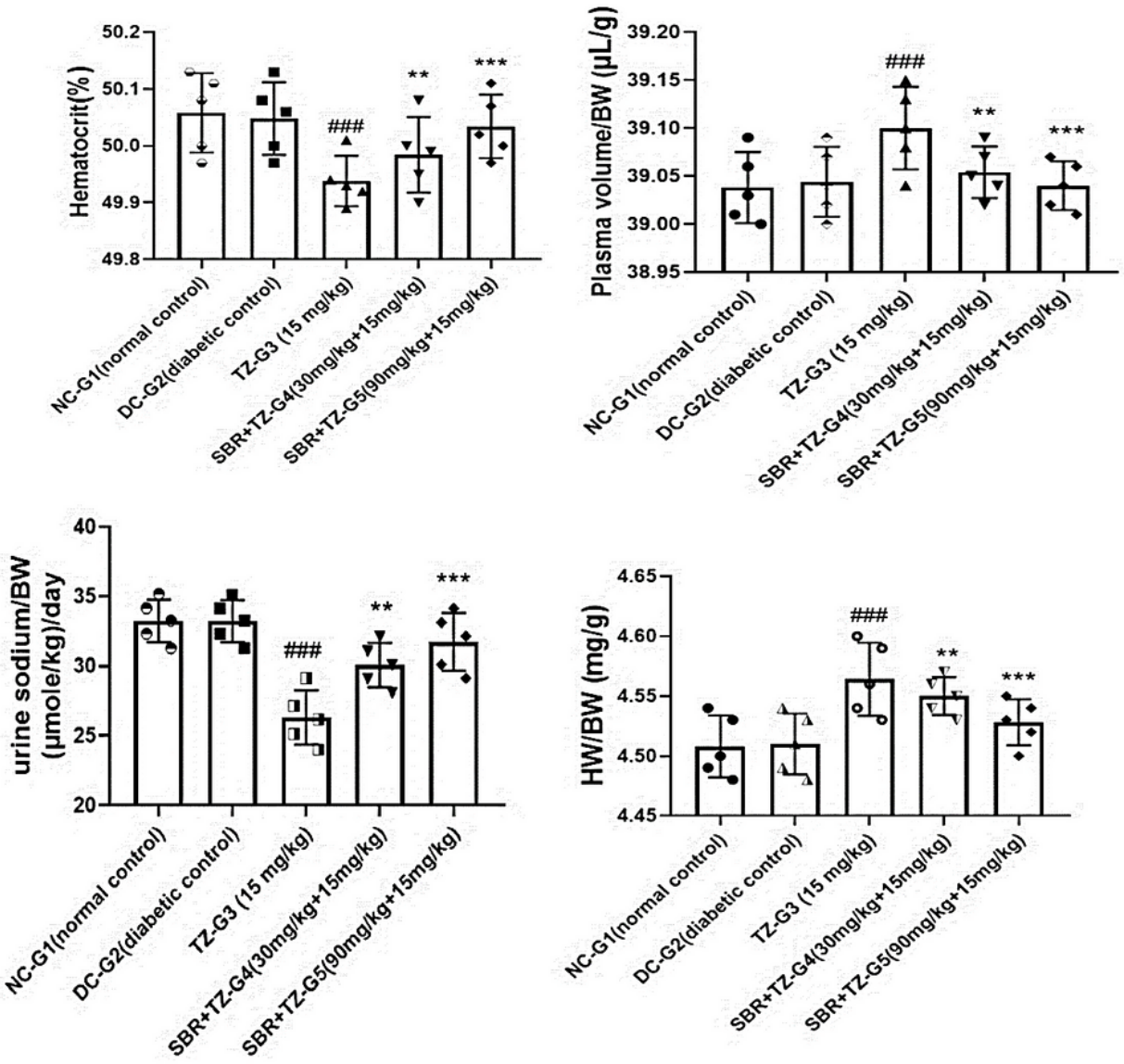

Figure 3

Effects of SBR co-treatments with TZ improved hematocrit, plasma volume/BW, HW/BW, and urine sodium/BW. Values are stated as means ± standard deviations of replicates, ** P < 0.01, *** P< 0.001, * P < 0.05 compared with the TZ-G2 group. ### P < 0.001 compared with control.

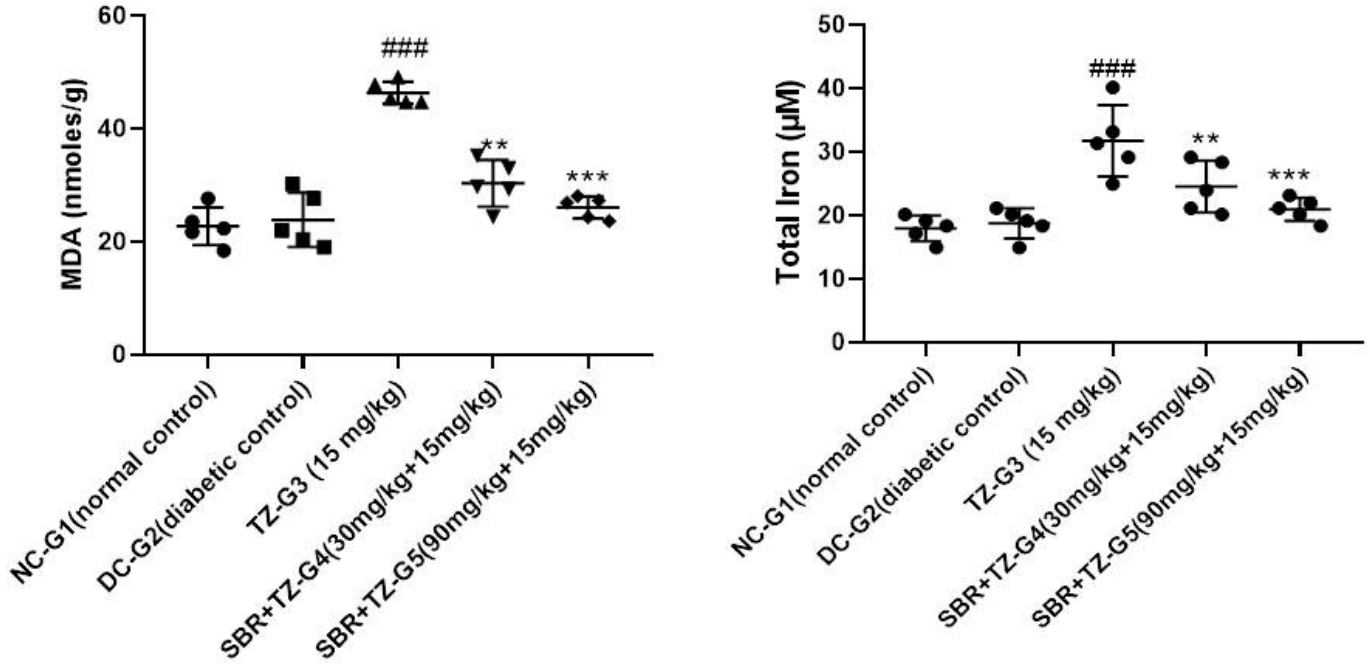

Figure 4

The co-treatments of SBR with TZ reinstated total iron concentration in serum and MDA level in heart tissues as compared to only TZ-treated rats. Values are stated as means ± standard deviations of replicates, ** $P < 0.01$, *** $P < 0.001$, ** $P < 0.05$ compared with the TZ-G2 group. $^{###}$ $P < 0.001$ compared with the control

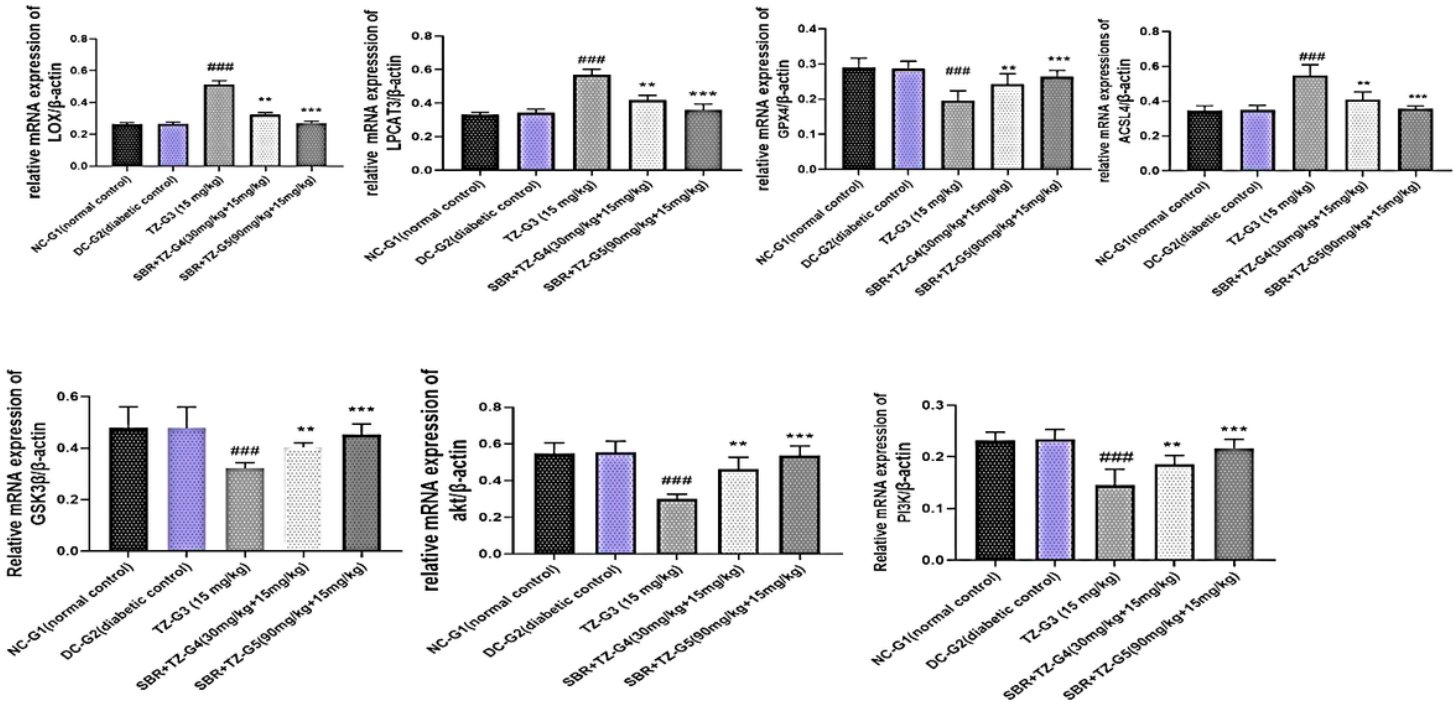

Figure 5

The co-administration of SBR and TZ were optimized relative mRNA expressions of mediators of ferroptosis (downregulated; LPCAT3, LOX, ACSL4: promoted; GPX4) and upregulated; P13K, AKT, GSK3β signaling pathways).

Values are stated as means ± standard deviations of replicates, ** $P < 0.01$, *** $P < 0.001$ compared with the TZ-G2 group. ### $P < 0.001$ compared with control.

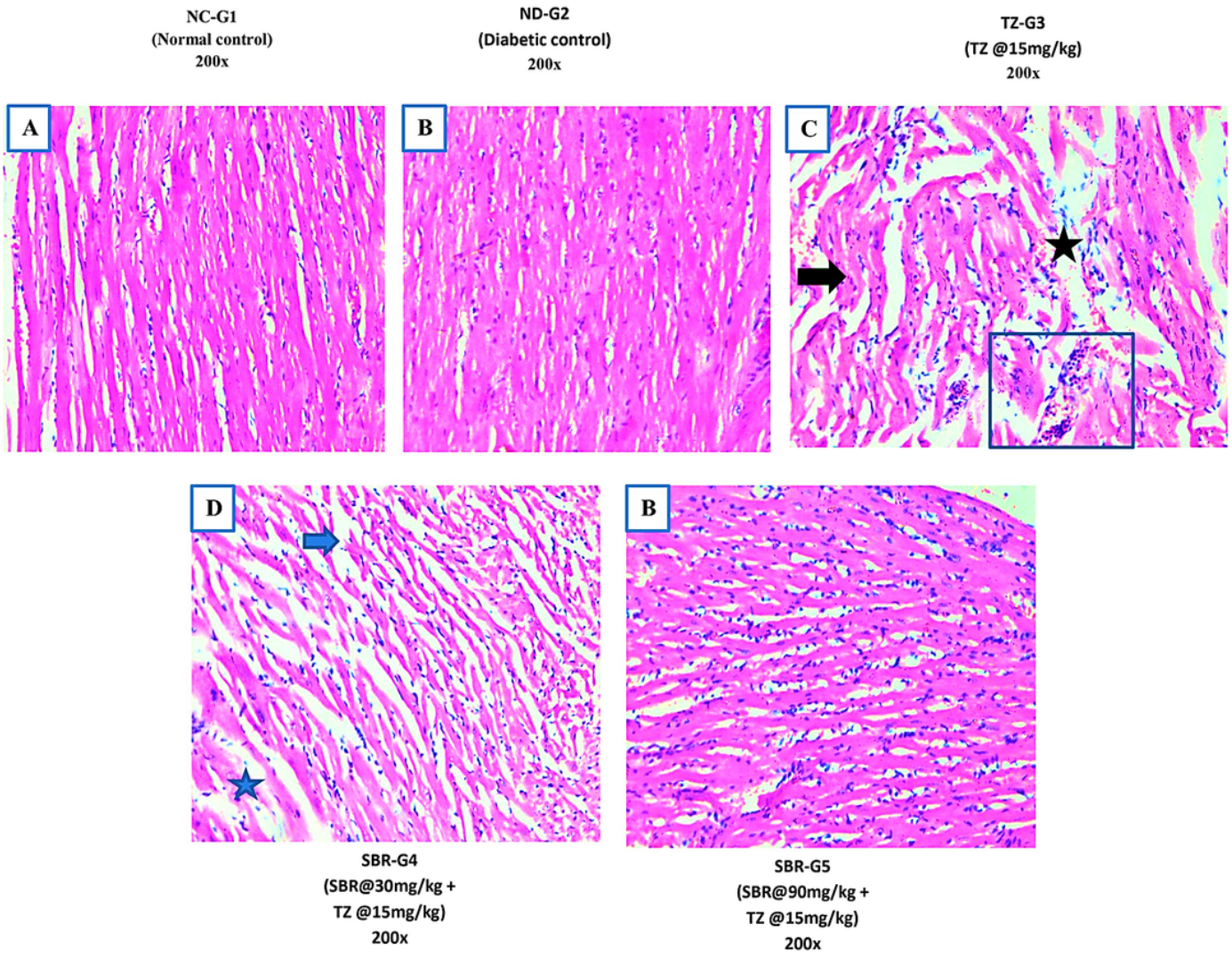

Figure 6

(A) Normal histological appearance of cardiac tissue of the control group, Bar: 50µm; **(B)** (200x): cardiac tissue of ventricle of a diabetic control rat showing normal histoarchiteture. Bar: 50µm; **(C)**: (200x) Cardiac tissue of the rat received TZ (15 mg/kg) shows wavy arrangements (black arrow), hypereosinophilia (blue box), and necrosis (black star). Bar: 50µm; **(D)** (200x) Ventricle histomicrograph of rats received cotreatments of SBR+TZ (30 mg/kg+15g/kg) exhibited reduced myocardial disarmaments and marked less necrosis (blue arrow) and cloudy swelling in cardiomyocytes (blue star), and **(E)** (200x) Ventricle histomicrograph of rats received cotreatments of SBR+TZ (90 mg/kg + 15 g/kg) are expressed normal arrangements of cardiomyocytes.